Chapter-7

Phosphorylation of sugarcane bagasse for the development of films and fruit foam for packaging of perishable food items

Motivation

Chapter 7 of this thesis delves into the innovative application of sugarcane bagasse (SB) for producing food packaging films and foam. This work aims to tackle the pressing concerns related to the improper disposal of this valuable agricultural waste. Despite its global presence, SB is frequently disposed of carelessly, such as improper landfilling or open burning, resulting in significant environmental damage. This chapter is driven by the urgent need to convert waste SB into valuable products, thereby reducing environmental damage and offering sustainable alternatives to traditional plastic packaging.

Key highlights

Development of a novel method for upcycling SB waste: *This chapter focuses on producing MFC gel from SB utilising a phosphorylation approach that is more ecologically benign than the expensive and environmentally harmful TEMPO-oxidation process.*

The utilisation of SB waste to add values in the food packaging area: *This chapter explores the potential of underutilized sugarcane by-product waste (SB) to extract cellulose, aiming to develop environmentally-friendly alternatives to traditional plastic-based packaging.*

Preservation of food products: *This chapter aims to address the need for sustainable packaging alternatives to reduce plastic-based environmental impact and preserve perishable food items, focusing on minimizing mechanical wear and tear of foods post harvesting and during food supply chain.*

Manuscripts under preparation:

1. *Rahul Ranjan, Chandra Kant and Prodyut Dhar Multifunctional cellulose phosphate-based food packaging films from biomass: Structure-functional relationship and environmental assessment studies. (**submitted to Food Hydrocolloids**)*
2. *Rahul Ranjan and Prodyut Dhar, Valorisation of agricultural waste: sugarcane bagasse as a source of aerogel and fruit foam for food packaging materials. (**To be submitted**)*

Graphical Abstract

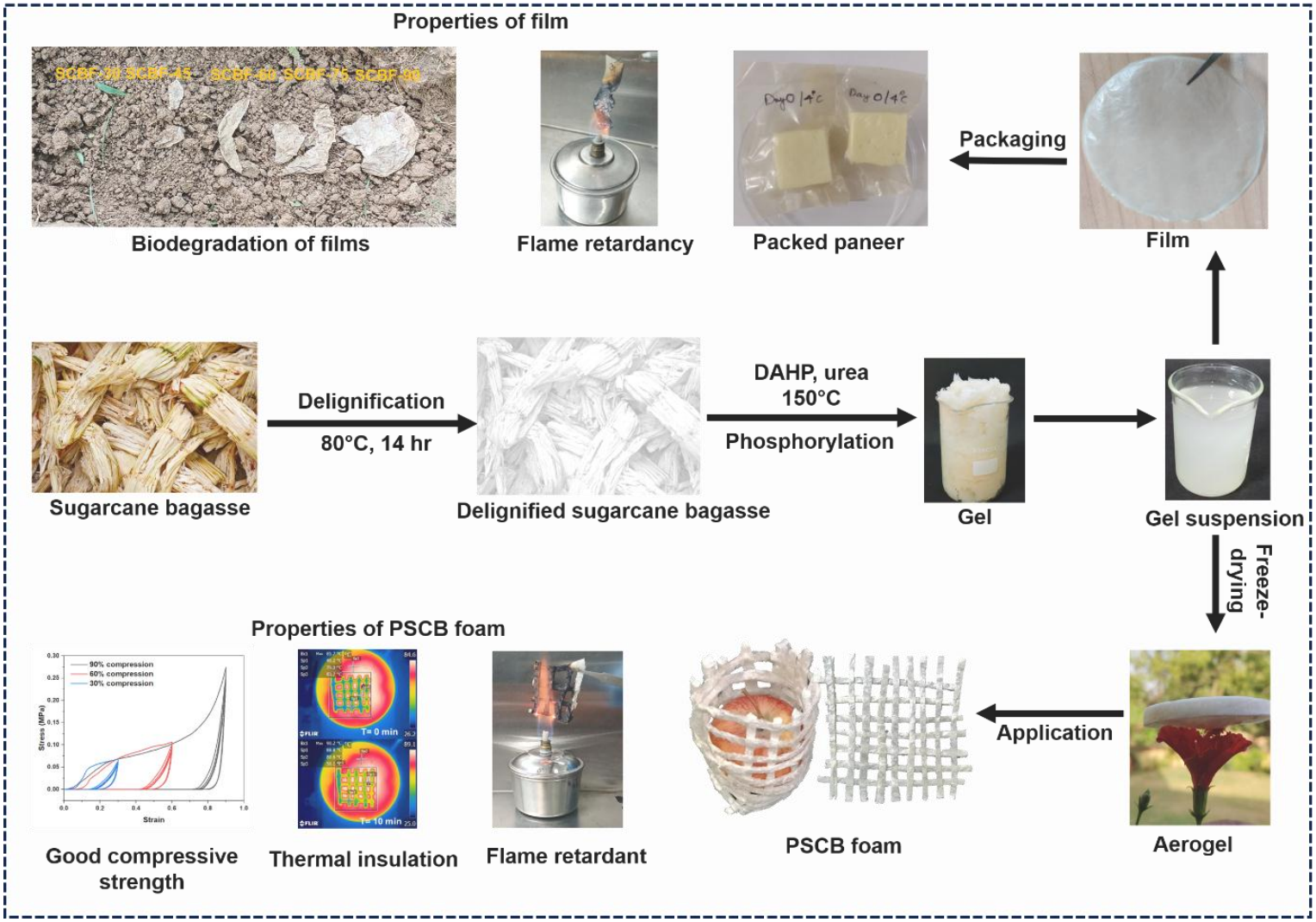

7.1 Introduction

Plastic packaging films have offered flexible and convenient solutions, which resulted in significant demand in the consumer-oriented world but led to various health, environmental, and sustainability challenges. These issues have prompted increased demand for biopolymers and biodegradable polymers such as cellulose, pectin, gelatin, chitosan, starch, polylactic acid, and polyhydroxy butyrate-based packaging material as an environmentally-friendly substitute [632]. Improper packaging of fresh fruit can lead to various forms of damage, such as wounds, peel cracks, and water loss, during transportation and handling. Fruits can undergo structural damage from mechanical stress, leading to moisture loss and the growth of harmful microorganisms [633]. This can damage the fruit's quality and raise concerns about food safety. Post-harvest handling can sometimes result in the deterioration of fresh fruits. The temperature of the environment plays a vital role in this process. Nowadays, fruits are wrapped in a foam mesh sleeve before being placed inside a box. The production of foam netting involves using polyethylene foam and expanded polystyrene [634,635]. It is commonly utilised for packing fruits because of its exceptional cushioning, excellent thermal insulation, shock absorption, and ability to maintain freshness. This can be a practical solution to address the issue of fruit loss during transportation [636]. However, there has been a growing restriction and legislation on using polyethylene foam and expanded polystyrene in recent years, mainly due to its adverse environmental consequences. The issue of food losses and waste has become a crucial concern in food management, with a specific emphasis on improving food security and reducing adverse environmental effects. Given the environmental and food security concerns, cellulose or cellulose-based foam netting could be a more favourable option for fruit packaging.

Sugarcane is a widely grown annual crop extensively utilised for sugar production and bioenergy applications. Sugarcane bagasse (SB) constitutes about 14-28 % of sugarcane plants, because of which it is generated in high-volume post-harvest, making it a widely available agricultural residue. SB primarily comprises cellulose, hemicellulose, and lignin, with cellulose being the most abundant component, accounting for 40% to 45% of bagasse fibres [637]. In recent years, cellulose from SB has been used for various applications such as thermal insulation, oil spill cleaning [580], heavy metals removal [638], sound absorbing material [639], packaging material [640], microbial fuel cell [641], biochar production, bioethanol [642], hydrogels [643], supercapacitor [644]. Over the years, this has been achieved through strategic chemical functionalisation of SB *via* amination [645], sulphonation [646], iodisation [647], TEMPO-oxidation [648], phosphorylation [245], *in-situ* modification using MoS_2 [649], graphene oxide [650], iron nanoparticles [638], TiO_2 nanoparticle [651] etc, converting the waste-to-value-added products for potential commercial applications. There is a significant opportunity to increase the worth of SCB by creating high-value products, providing economic benefits and contributing to its renewable characteristics.

This chapter examines using sugarcane bagasse (SB) waste as a valuable resource for developing sustainable packaging solutions. By employing a highly effective and environmentally friendly method that combines delignification and phosphorylation, cellulose phosphate gels achieve a remarkable yield of over 85%. These gels exhibit varying charge composition and colouration according to their curing duration. These gels produce films using the solution cast technique, improving mechanical strength, thermal stability, and flame resistance. The films produced demonstrate exceptional water resistance and comply with migration limitations. A life

cycle study has additionally validated a reduction in CO_2 emissions, affirming the eco-friendly characteristic of the procedure. Furthermore, the utilisation of gel-sealed films serves to extend the duration of packed paneer's storage by inhibiting bacterial proliferation and lipid oxidation. Furthermore, freeze-drying processes can transform phosphorylated cellulose gels from SB into flame-retardant foams. These foams possess exceptional characteristics, including high porosity, low heat conductivity, and strong mechanical stability. These foams have been expressly engineered to package fruit, specifically apples. They offer packing alternatives that are both lightweight and thermally stable. Essentially, this comprehensive strategy provides a solution for utilising SB trash to produce environmentally acceptable packaging materials, address environmental concerns and enhance food preservation and safety. This chapter has been divided into two subsections**. Section 7.2** discusses the application of SB films as packaging material for fruits. In contrast, **section 7.3** focuses on applying SB foam for packaging apples.

7.2 Results and discussion

SB has recently attracted wide attention in commercial food packaging as an alternative to plastics due to their low-cost, biodegradability, non-toxicity and abundance lignocellulosic availability. The current study presents the fabrication of packaging films from SB *via* delignification and phosphorylation based functionalization route. During phosphate modification, disintegration along with introduction of phosphate groups to cellulose backbone occurs resulting in transition to gel-like structure. The produced gels show tuneable CC of~500 to 1033 mmol/kg depending upon curing time~ 30-90 minutes which also resulted in variation of colour from white to pale yellow (***Figure 7.1***). After phosphorylation, gels were further

homogenised, sonicated and casted to produce flame-retardant, transparent, mechanically robust biodegradable films with low wettability. The films were evaluated for migration under various simulated conditions and used for packaging of perishable milk-based products such as paneer, which improved the shelf life upto 14 days. The present work is a scalable approach for valorization of abundantly available SB waste into value-added packaging with improved physiochemical, functional and structural properties making it a promising alternatives to non-degradable plastic-based packaging.

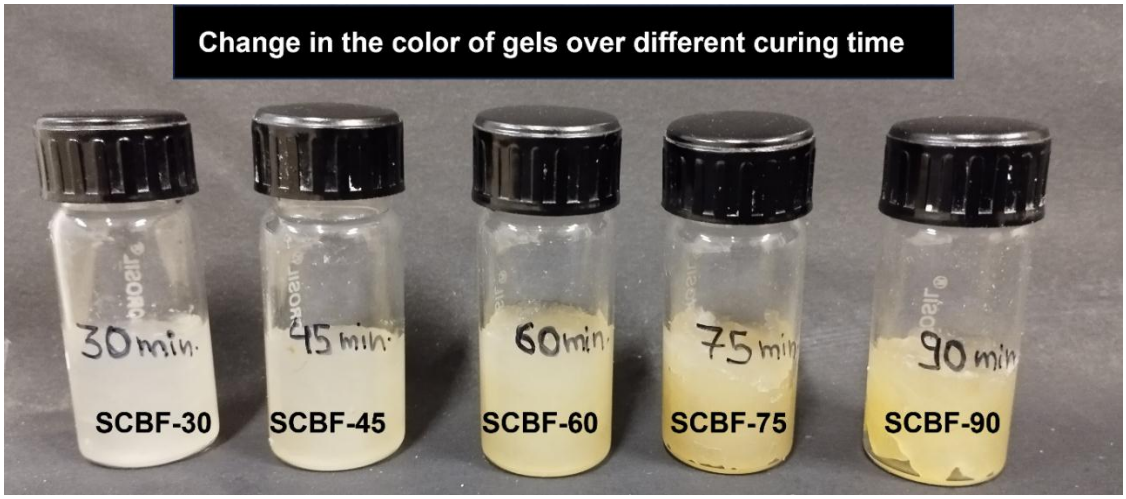

Figure 7.1 *Colour of gels produced at different curing times with DAHP and urea at 150 °C.*

7.2.1 Physiochemical properties of the films

7.2.1.1 Evaluation of charge content

Conductometric titration was performed to determine the abundance of phosphate charge in the prepared films at different curing times. ***Figure 7.2*****(a-e)** shows the conductometric curves which were found to be divided into three regions. The first region corresponds to the highly acidic groups due to presence of excess H^+ ions, responsible for decrease in conductivity on addition of NaOH. The second portion

corresponds to the stagnant region where neutralisation of proton of phosphate groups takes place, and the volume of NaOH consumed in this region was used to calculate the CC. The third section of conductivity curves indicates -OH group abundance, as also observed in the previously reported studies [225,652]. All the films exhibit a plateau region in their conductivity curves, and the length of this plateau increases as the curing time is extended. The SCBF-90 film produced after curing of 90 minutes, exhibited the highest CC of~1033.3 mmol/kg. As the curing time increased CC also increased gradually in films with SCBF-30 ~500 mmol/kg, SCBF-45~566 mmol/kg, SCBF-60 ~700 mmol/kg and SCBF-75 ~ 900 mmol/kg respectively. The progressive increase in CC with longer curing times suggests substitution of hydroxyl groups in cellulose backbone with phosphate groups which were further confirmed through FTIR and XPS spectroscopic studies, as discussed in subsequent sections.

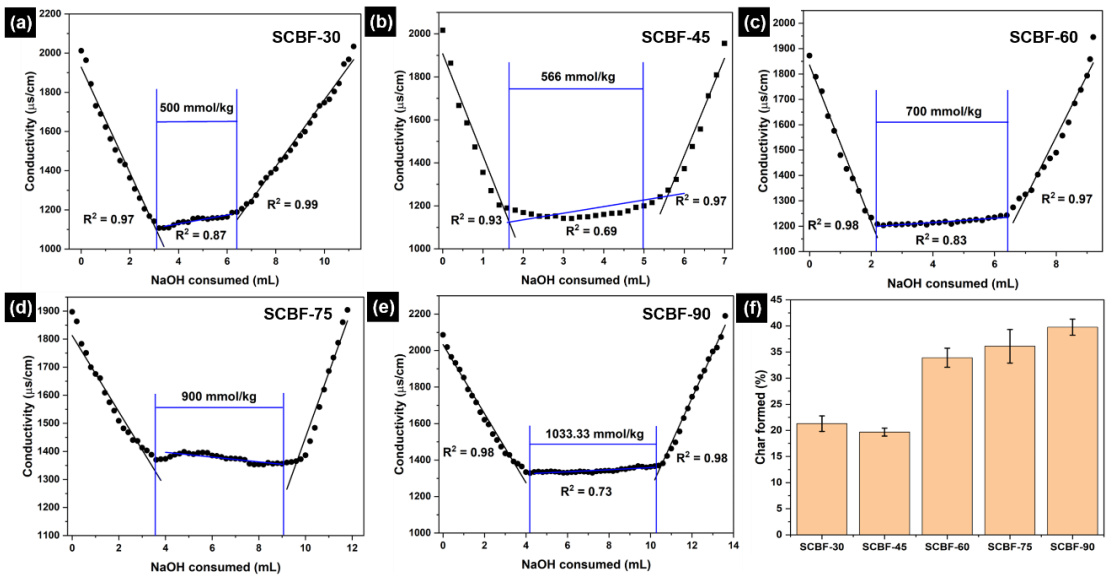

Figure 7.2 *Charge content of the film produced after different curing times (30-90 minutes) (a) SCBF-30, (b) SCBF-45, (c) SCBF-60, (d) SCBF-75, (e) SCBF-90 and (f) the char residue formed after the flame test of the films.*

7.2.1.2 FTIR spectra analysis of phosphorylated SB films

FTIR analysis was carried to investigate the changes in chemical functionalization after the delignification and phosphorylation process. ***Figure 7.3*(b)** shows full range FTIR spectrographs with IR peaks at 666 cm^{-1}, 898 cm^{-1}, 1023 cm^{-1}, and 1108 cm^{-1}, which corresponds to specific molecular vibrations, namely C-C bending, C–O stretching of β-(1–4) glycosidic linkages, C-O-C bonds, and stretching vibration of pyranose ring, respectively (25–28). The IR peaks observed at 1308 cm^{-1}, 1371 cm^{-1}, 2880 cm^{-1}, and 3340 cm^{-1} in ***Figure 7.3*(a)** and ***Figure 7.3*(b)** correspond to C-H deformation, -CH_2 bending, -C-H stretching, and O-H stretching, respectively [630,652,657,658]. FTIR of SCBF film shows presence of three additional IR peaks at ~828 cm^{-1}, 1103 cm^{-1}, and 1240 cm^{-1}, which confirms presence of P-O-C and P=O vibrational bonds respectively inline with the previously reported studies (Radiman and Rifathin, 2013; Suflet et al., 2006; Zhang et al., 2023; Jiang et al., 2012). The introduction of phosphate ions into DSB resulted in formation of P-O-C bonds, facilitating the covalent linkages of phosphate groups with the cellulose backbone which was further confirmed through XPS studies.

7.2.1.3 XPS analysis of DSB and SCBF

XPS analysis was performed to confirm the formation of covalent linkages and crosslinking during phosphorylation reaction. The XPS survey of DSB exhibited two distinct peaks at 533.08 eV and 285.08 eV, which attributes to *O1s* and *C1s* bonds, respectively (***Figure 7.3*(c)**). In case of SCBF-60 (***Figure 7.3*(c)**), the XPS shows three distinct peaks at 532.08 eV, 285.08 eV, and 133.08 eV, corresponding to the *O1s*, *C1s*, and *P2p* chemical bonds, respectively. In the present study, the *C1* broad spectrum of

DSB (***Figure 7.3*(d)**) resolved into three subpeaks at the binding energies of 284.3 eV, 286 eV and 287.3 eV, representing C-H/C-C, C-O and O-C=O bond respectively [660,661]. The broad spectrum of *C1s* in SCBF-60 ((***Figure 7.3*(d)**),) also resolved into three distinct sub-peaks at 284.3 eV, 285.8 eV, and 287.0 eV, corresponding to the C-C, C-OH, and C-O bonds, respectively [601,662]. The broad spectrum of *O1s* (DSB, (***Figure 7.3*(e)**)), deconvoluted into three subpeaks at 530.6 eV, 532.3 eV and 532.8 eV, which depicts C=O, -O-H, and C-OH bonds respectively [663–665]. However, on phosphorylation, the *O1s* peak of SCBF-60 at 530.8 eV, 532.2 eV and 533.4 eV represents P=O, -P-O, and C-O/P-O bonds respectively ***Figure 7.3*(e)**) [666–668]. The *P2p* broad spectrum of SCBF-60 (***Figure 7.3*(f)**) also divided into three subpeaks at 133.5 eV, 134.7 eV and 132.7 eV, corresponding to P=O, O=P-O and P-O, respectively [669–671]. However, no peaks were observed in the DSB sample for *P2p* (***Figure 7.3*(f)**). The presence of phosphate bonds in *O1s* and *P2p* spectra of SCBF-60 confirms the grafting of phosphate groups in DSB backbone. The elemental composition of SCBF-60 shows presence of phosphate at~ 1.7 atomic %, which is inline with the charge determined through conductometric titration and EDX spectroscopic studies.

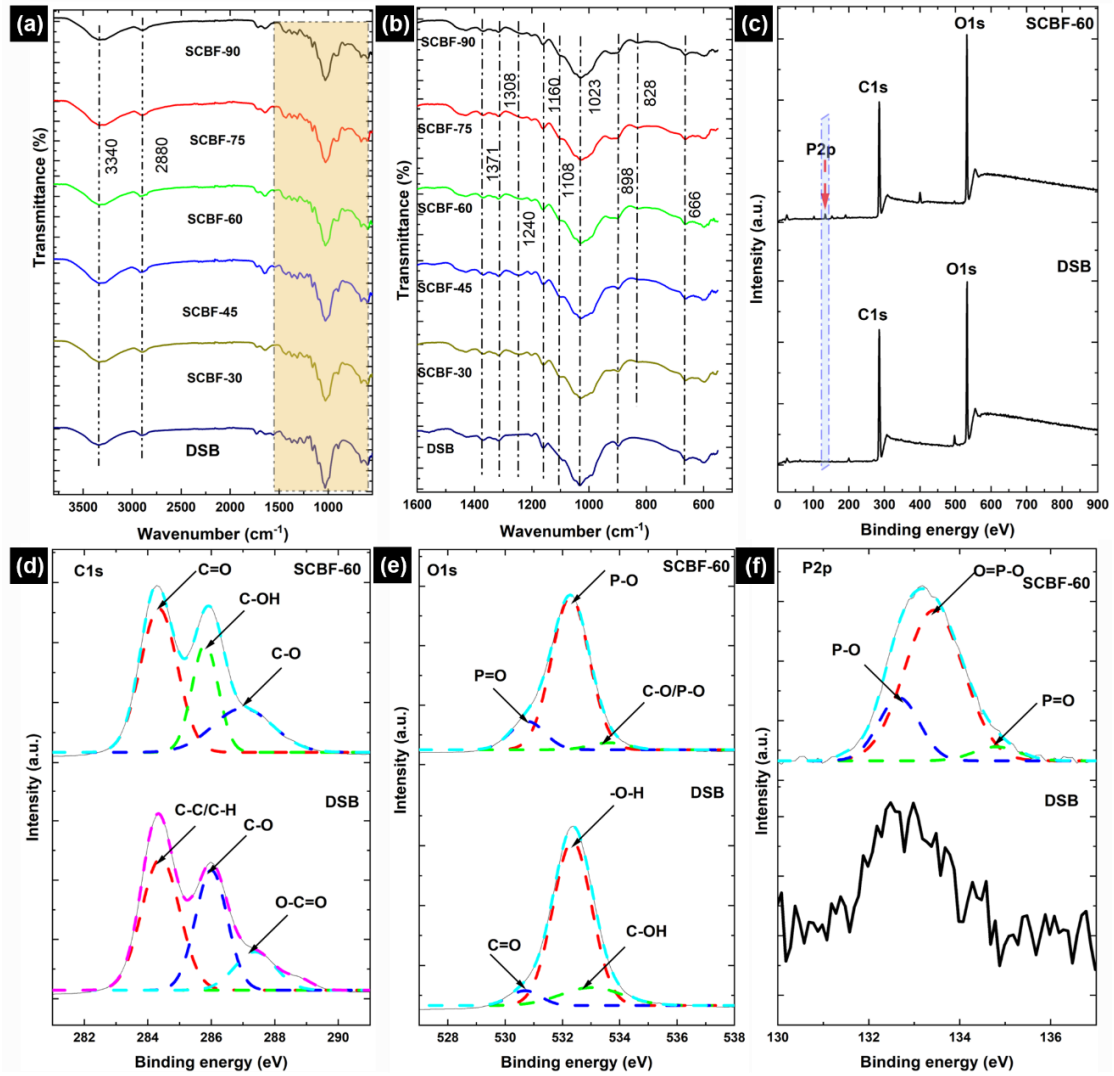

Figure 7.3 *FTIR spectra (a) in the range of 600-4000 cm^{-1}, (b) 600-1600 cm^{-1}, (c) XPS survey of DSB and SCBF-60, (d) C1s, (e) O1s, and (f) P2p bond of DSB and SCBF-60.*

7.2.2 Morphological properties of phosphorylated SCB films

SEM analysis was performed to investigate the surface morphology of developed films, as shown in ***Figure 7.4***. The SEM images of SCBF-90 (***Figure 7.4*****(a-d)**) exhibit random distribution of cellulose fibrils with formation of uneven and rough surface. The uneven distribution of fibrils with irregular structures in films can be attributed to disintegration of fibre's structure during homogenisation ***Figure 7.4*****(a)** and ***Figure 7.4*****(b)**. The solution casting of prepared gels and heat-induced drying process resulted in a continuous and dense cellulose film layer. The presence of network

structure of cellulose fibrils with formation of densified system without any voids spaces is expected to improve the structural properties of films, as discussed in subsequent section. The results of EDS analysis and elemental mapping performed on SCBF-90 film are depicted in ***Figure 7.4*(e).** The elemental mapping shown in ***Figure 7.4*(f), *Figure 7.4*(g),** and ***Figure 7.4*(h)** shows spatial distribution of phosphorous, carbon, and oxygen elements on films surface confirming the uniform phosphorylation and distribution on DSB surface. EDS spectra shows the presence of phosphate with a weight percentage of 9.37%, which is inline with the XPS and conductometric titration as discussed in earlier section.

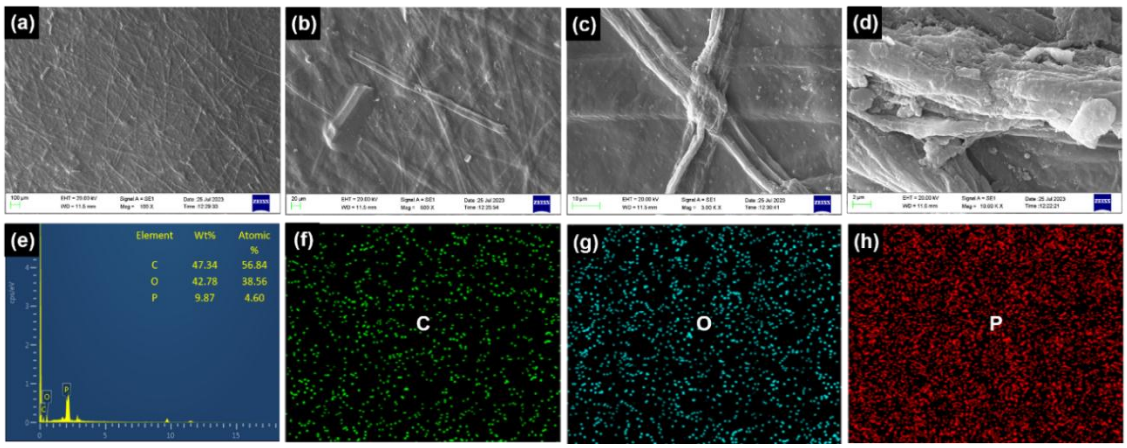

***Figure 7.4** SEM micrograph of SCBF film (a)100x, (b)500x, (c) 3kx, and (d) 10kx, (e)EDS analysis with elemental mapping of (f) carbon, (g) oxygen, and (h) phosphorous, respectively.*

7.2.3 Structural properties of phosphorylated SCB films

XRD was carried out to analyse the structural changes in DSB during delignification and curing based phosphorylation and film formation process. As shown in ***Figure 7.6*(a)**, two characteristic peaks of cellulose were observed in DSB at 15.1° and 21.5°, representing the crystal plane (1-10) and (200), respectively [672,673]. After the phosphorylation reaction, shift in peaks were observed with peak at 15.1° of DSB

shifted to 16.2° and 21.5° to 22.4°, representing (110) and (200) plane of cellulose, respectively [674,675]. The crystallinity index (*C.I*) of DSB and SCBF-30 was 38.3% and 38.9%, indicating that there was no significant effect of curing time on crystallinity for first 30 minutes. Furthermore, with the increase in phosphorylation time from 45 to 75 minutes there was no observable change in C.I. ~41.9%, 42.4% and 42% for SCBF-45, SCBF-60, and SCBF-75 respectively. The phosphorylation process leads to incorporation of significant amount of phosphate groups into the amorphous region of DSB, without affecting the crystallinity significantly [652]. However, following a more extended curing period to 90 minutes C.I. reduced to 32.3% possible due to significant swelling and partial dissolution of DSB fibres leading to degradation, as also observed in previously reported studies [255,595].

7.2.4 Thermal properties of phosphorylated SCB films

To understand the effect of delignification and phosphorylation thermogravimetric analysis was carried for developed SCBF films at different curing time as shown in ***Figure 7.6*****(b)**. The first stage of weight loss~6.32 %, 3.56 %, 3.55 %, 4.57 %, 3.7 % and 5.1 % was observed in 30-105°C range for DSB, SCBF-30, SCBF-45, SCBF-60, SCBF-75 and SCBF-90 respectively. The onset thermal degradation temperature (T_{onset}) were observed at 235 °C for DSB which decreased with increasing curing time to 223 °C for SCBF-30, 231°C for SCBF-45, 215°C for SCBF-60, 230°C for SCBF-75 and 213°C for SCBF-90. DSB demonstrates two stages of decomposition; first stage with 51.03 % degradation occurred in temperature range from 232-336°C and second stage with 19.15 % degradation observed from 430-548°C. T_{max} of DSB was found to be 318°C which on phosphorylation improved to 555°C, 427°C, 438°C, 455°C and 423°C for SCBF-30, SCBF-45, SCBF-60, SCBF-75 and SCBF-90

respectively. The residual weight percentage of SCBF-30, SCBF-45, SCBF-60, SCBF-75 and SCBF-90 at 700°C were 37.71%, 38.96%, 39.27%, 41.22% and 45.48% respectively which significantly increased incomparision to DSB with 6.67%,. The results indicate that incorporation of phosphate groups increased the yield of char residues in all films at different curing time, inline with findings reported in previous works [225,237,245].

7.2.5 Mechanical properties of phosphorylated SCB films

The evaluation of mechanical properties of SCBF films with different CC (***Figure 7.6*(c)** and ***Figure 7.6*(d))** were performed to determine the strength and modulus under applied tensile load. SCBF-30, SCBF-45, SCBF-60, and SCBF-75 films shows a tensile strength of 24.05, 38.37, 37.58 and 39 MPa, respectively. Interestingly, SCBF-90 films show an increase in tensile strength by almost two orders of magnitude to 55.80 MPa. The increased tensile strength could be attributed to enhanced crosslinking of phosphate groups during thermal induced processing which improves the load bearing capacity of films. Similarly, due to higher elongation SCBF-75 films shows improved modulus of 1098.79 MPa followed by 1017.59 MPa for SCBF-45, 886.04 MPa for SCBF-30 and 817.58 MPa for SCBF-90 films. The cellulose films are known for their poor stability under wet conditions, however, the presence of cross-links improve wet stability of films. In comparison to dry films, the wet strength reduced to 5, 4, 6, 9 and 10MPa for SCBF-30, SCBF-45, SCBF-60, and SCBF-75 films respectively, but are suitable enough for practical application**s (*Figure 7.5*(a)).** The high degree of phosphate CC and their subsequent cross-linking during processing of SCBF films [252] significantly improves strength both in dry and wet conditions, overcoming challenges associated with traditional cellulose-based packaging films.

7.2.6 Water absorption capacity of phosphorylated SCB films

In packaging applications, understanding water absorption capacity and water solubility of developed cellulose films is vital to evaluate their ability to act as barriers against moisture. In this study, water absorption capacity of films decreased with an increase in degree of phosphorylation and crosslinking in films. From ***Figure 7.6*(e)**, SCBF-30 shows maximum water absorption capacity of 2016.8% which reduced to 1333%, 939.94%, 801.43%, and 525.77% for SCBF-45, SCBF-60, SCBF-75, and SCBF-90 films, respectively. Upon exposure to water, SCBF films with phosphorylated groups exhibits a propensity to interact with water, however, presence of crosslinking restricts water infiltration reducing its water absorption. It is also evident from reduced water solubility of SCBF films~15-18% (***Figure 7.5*(b))**, when immersed in water for 24 hours. Moreover, the wet SCBF films shows structural integrity and improved wettability in comparison to traditional cellulose films, as discussed in subsequent expansion.

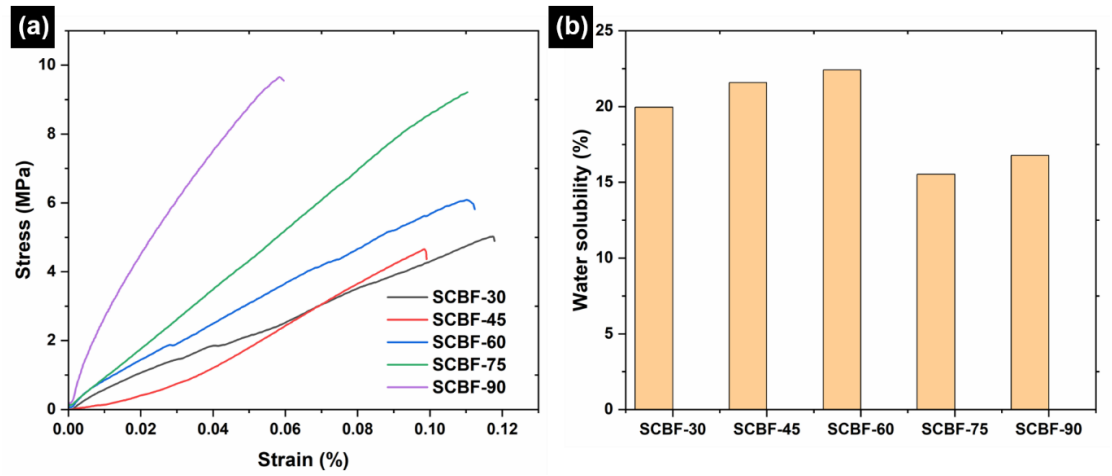

***Figure 7.5** (a) Tensile strength and (b) water solubility of phosphorylated SCB film in wet condition*

7.2.7 Surface wettability of the phosphorylated SCB films

The surface wettability of packaging films were studied by measuring water contact angle (CA) over a time-period to evaluate their behaviour when in contact with food. As shown in ***Figure 7.6*****(f),** SCBF-60 shows highest initial CA of 68.88°, which almost remains unchanged with varying CC of films to 68.46°, 65.61°, 67.37° and 67.31° for SCBF-30, SCBF-45, SCBF-75 and SCBF-90 respectively. However, final CA after 5 minutes was found to vary depending on curing time which reduces the wettability of films, due to introduction of thermal induced cross-linkages. The final CA was found to be 17.70°, 20.33°, 30.05°, 24.99° and 26.49° for SCBF-30, SCBF-45, SCBF-60, SCBF-75 and SCBF-90 films. From SEM observations, SCBF films showed a rough architecture with cellulose microfibrils on surface, which led to easy adsorption of water droplets through capillary action. Alongwith it presence of hydrophilic phosphate groups led to spreading of water droplets with reduction in final CA of films with time. Increase in curing time leads to crosslinking of phosphate groups, which diminishes interaction of hydrophilic phosphate groups with water droplets thereby reducing wettability and improving CA, making the prepared SCBF films suitable for food packagings.

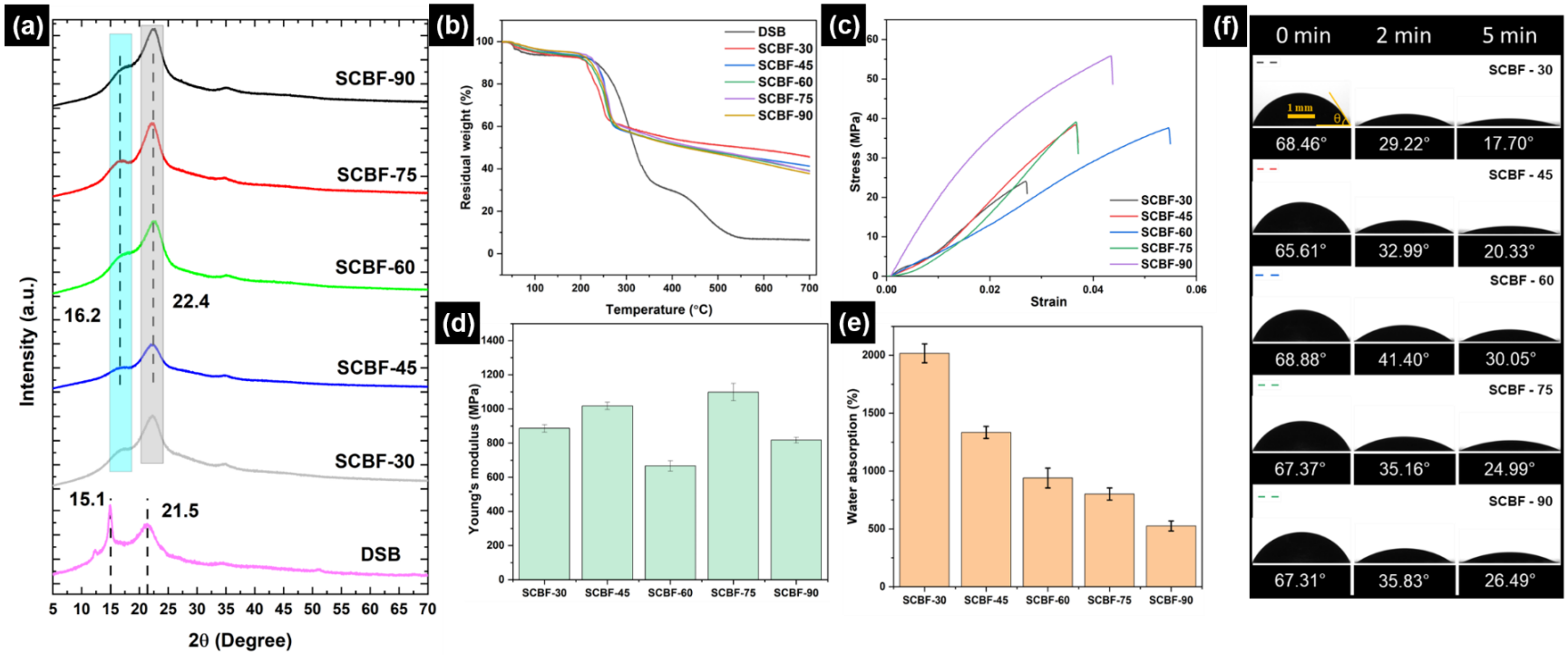

Figure 7.6 *(a) XRD diffractogram, (b) thermogravimetric analysis, (c) tensile strength, (d) tensile modulus, (e) water absorption capacity, and (f) contact angle.*

7.2.8 Flammability

The flammability test were carried out on exposing films under direct ethanol flame to determine film's susceptibility to ignition, rate of burning and characteristics of char residue formed at end of test. As depicted in ***Figure 7.7***, films such as SCBF-30, SCBF-45, and SCBF-60 catches fires quickly (2-5 seconds), and the burning rate was ~ 2.66-1.6 cm/min. However, SCBF-75 films shows improved flame retardancy with slow burning upto 15 seconds, and reduced burning rate of 0.571 cm/sec, by almost two orders of magnitude. The burning rate further reduced maximum for SCBF-90 (0.15 cm/sec), possibly due to the highest phosphate charge (1033.33 mmol/kg). During burning of films, the surface becomes black with formation of char however retain its dimensional and structural integrity. The char residue left after flammability experiments were 21.28, 19.7, 33.9, 36.9 and 39.7% for SCBF-30, SCBF-45, SCBF-60, SCBF-75 and SCBF-90, respectively, which is inline with TGA studies, discussed in previous section.

7.2.9 Migration studies of phosphorylated SCB films

For food packaging films, integrity in terms of leaching of components is an essential criterion for study as it may affect the sensory properties of packed food items. Migration studies were performed with two food simulants, namely ethanol (alcoholic food simulant) and isooctane (fatty food simulant), following EU regulation No. 10/2011(***Figure 7.8*****(a)**). For ethanol as a simulant, overall migration of SCBF-45, SCBF-60, SCBF-75 and SCBF-90 shows 45569, 37130, 35443, and 30379 µg/kg, which increased to 60759 µg/kg for SCBF-30. The migration decreased with increase in phosphate charge groups in films, due to the formation of heat-induced cross-linkages which improves their wet stability. On other hand, SCBF-30 films with low

CC underwent swelling followed by disintegration due to absence of such crosslinks during incubation for 10 days. However, the migrated components are mostly cellulosic fragments which are known to be biocompatible and non-toxic in nature. Similar observation with significantly lowered migration values were detected with isooctane as a non-polar solvent. The overall migration decreases with increased phosphate content as higher phosphate groups improve crosslinking ability between cellulose fibrils, resulting in lower swelling and disintegration on exposure to solvent [24]. Moreover, all the films (except SCBF-30 in ethanol) showed migration values within the EPA standard limit (60,000 micrograms/kg) and can be confirmed suitable for food packaging applications.

7.2.10 Packaging of the paneer and evaluation of their shelf life

The biodegradable food packets of SCBF-90 films with dimensions ~5 cm × 1.5 cm were fabricated, which were utilized for packaging paneer at 4°C for 21 days (shown in ***Figure 7.8*****(e))**. Under packed conditions, the colour of paneer changed from natural white to lighter shade of yellow in both control and packaging conditions depending upon storage time. Furthermore, an alteration in consistency of paneer was noted as it transitioned from soft and spongy to more rigid form in case of control sample within 7 days of storage time. In contrast, paneer under packed condition remained soft and spongy even after 21 days of storage.

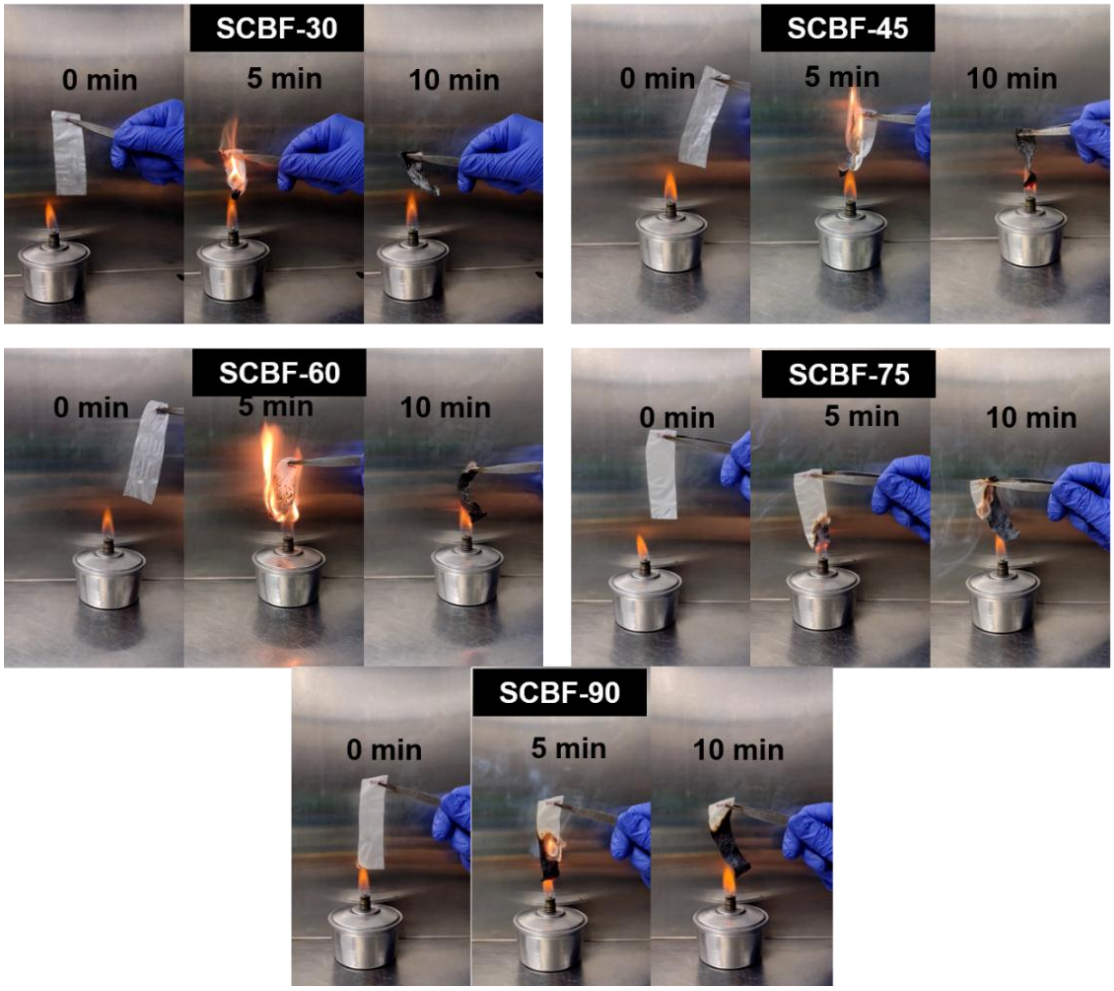

Figure 7.7 *Evaluation of flame-retardant properties of the SCBF-films*

During 21 days of storage period, a change in pH was observed from 5.6 to 6.8 in control, whereas negligible change was observed in packaged samples (***Figure 7.8*****(b))**. Furthermore, there was an increase in peroxide value of paneer from 1.52 to 2.60 mmol/kg in control after 14 days, however, packaged samples shows slight increase in peroxide value from 1.52 to 1.64 mmol/kg even after 21 days of storage time (***Figure 7.8*****(b))**. Microbiological evaluations were performed on samples collected at different time intervals (0, 7, 14, and 21 days) to evaluate growth of potentially harmful pathogenic bacteria that could affect human health. The investigation involved assessment of growth of lactic acid and coliform bacteria by

using selective MRS and VRBA agar plates, respectively. According to data in ***Figure 7.8* (d)**, the control sample exhibited 3.38, 3.67, 3.76, and 3.69 log CFU/g of lactic acid bacteria after being stored for 0,7,14 and 21 days, respectively. On other hand, packaged samples showed reduced growth of lactic acid bacteria with 2.30, 2.84, 2.90, and 2.47 log CFU/g under identical storage durations. Significantly, the selective VRBA, XLD agar and PALCAM agar plates exhibited no detectable growth of pathogenic coliform bacteria, *Salmonella* and *Listeria* species during entire 21-day of storage period. Additionally, absence of *Pseudomonas* species was confirmed as there was no observable growth on the *Pseudomonas* agar plates, as depicted in ***Figure 7.11***. There were no visible growth of yeast or fungi in samples stored until 14 days in PDA agar. However, it was observed that both control and packaged samples exhibited growth of 3.30 and 3.11 log CFU/g of yeast/fungus only after 21 days of storage, respectively (***Figure 7.8*(c)** and ***Figure 7.8*(d)**). This implies that the developed SCBF-90 films when used for packaging of paneer could maintain its suitability for consumption upto 14 days.

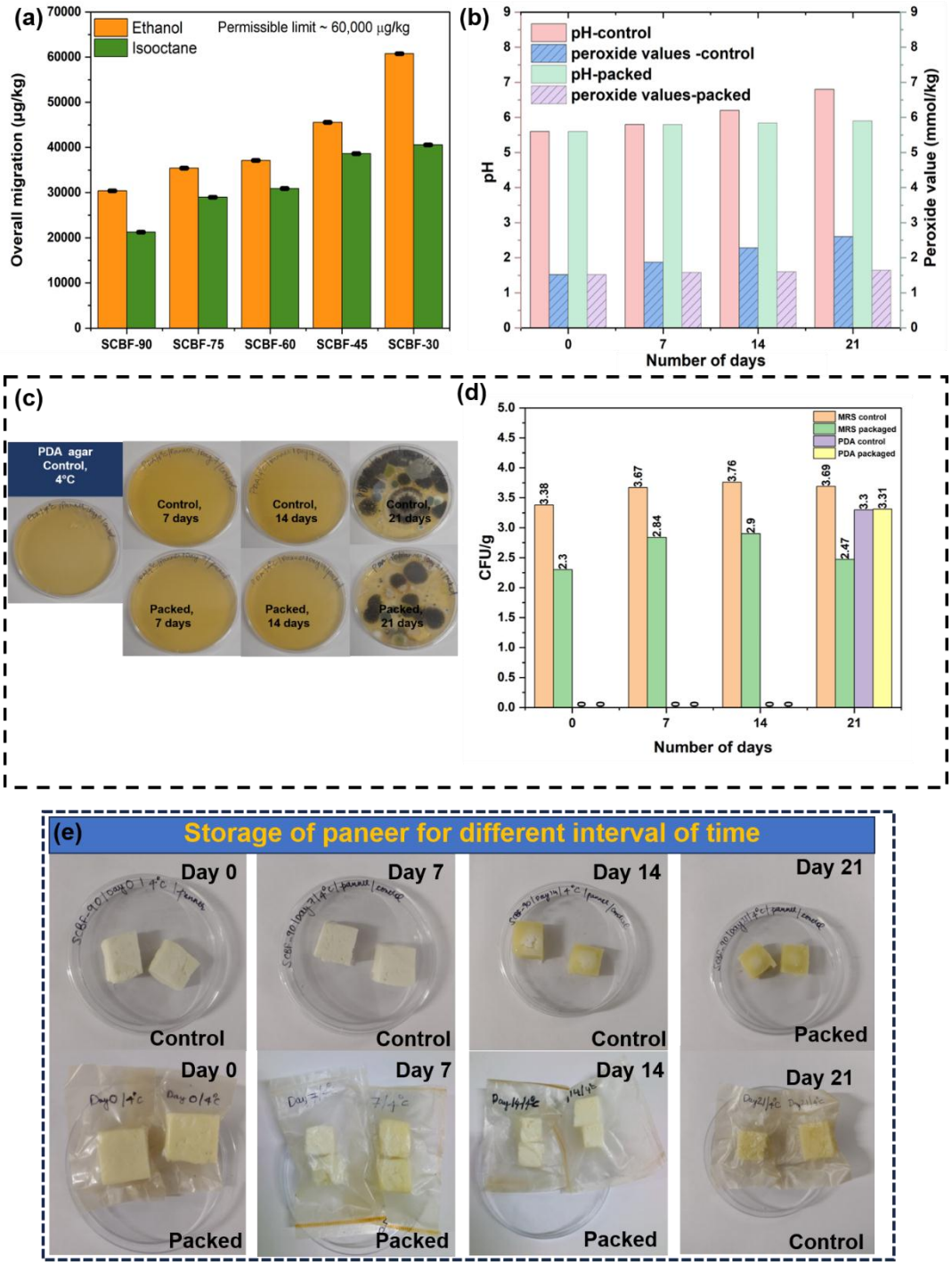

Figure 7.8 *(a) Overall migration values measured in presence of food simulants ethanol and isooctane, (b) changes in pH and peroxide values for control and SCBF films packed paneer, (c) PDA agar plates for growth of yeast/fungi at different time period, (d) measured colonies in presence of MRS/PDA agar media, (e) changes in colour and texture of paneer stored under control and packaged conditions at different storage time upto 21 days at 4 °C.*

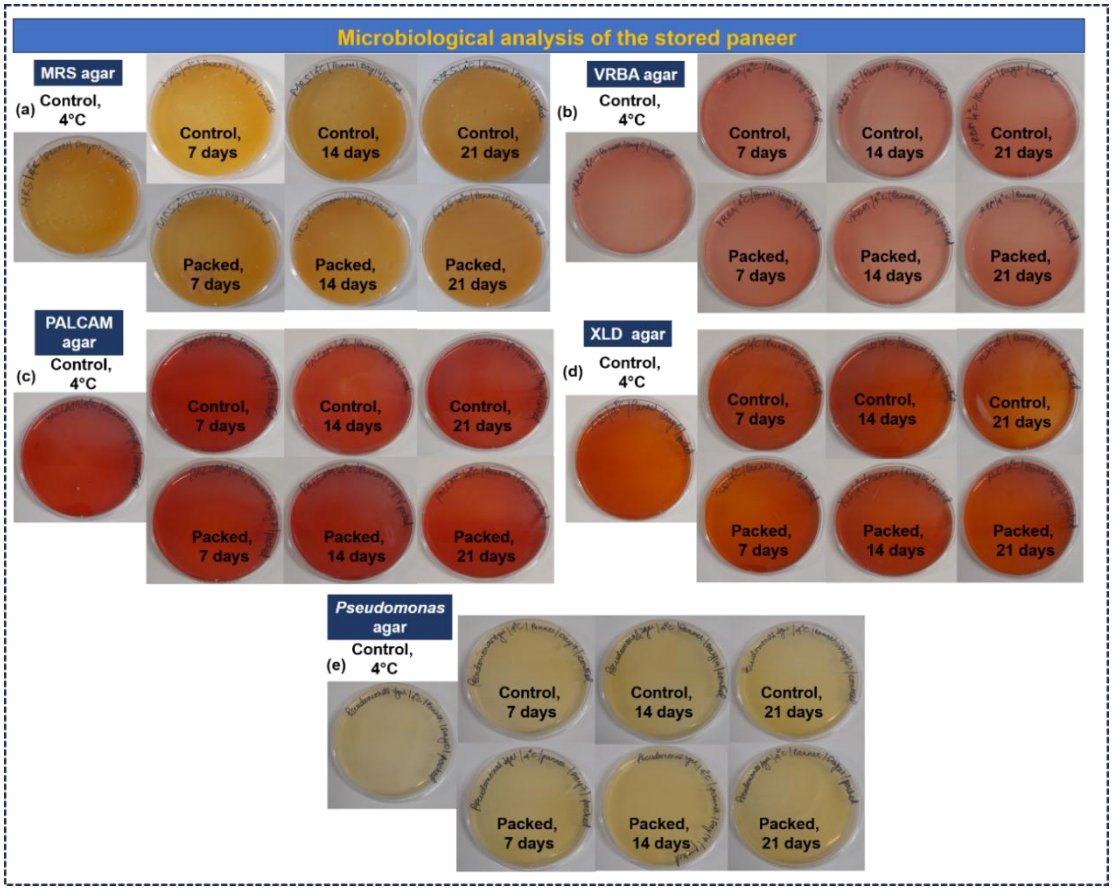

Figure 7.9 *(a) Microbiological analysis of the packaged and control samples in de Man, Rogosa and Sharpe (MRS) agar, Violet Red Bile agar (VRBA) agar, Polymyxin Acriflavin Lithium-chloride Ceftazidime Esculin Mannitol (PALCAM) agar, Xylose Lysine Deoxycholate (XLD) agar and Pseudomonas agar.*

7.2.11 Biodegradation of phosphorylated SCB films

However, after 28 days of burial all films underwent significantly increased biodegradation leading to observable disintegration **(*Figure 7.10*(d)** and ***Figure 7.10*(j))**. After 28 days the biodegradation of SCBF-30 and SCBF-45 were 99.55% and 87.56 receptively. On the other hand, SCBF-60, SCBF-75, and SCBF-90 films demonstrated lowered biodegradation of 72.60%, 56.67%, and 29.72%, respectively, following 28-day burial period. The SCBF-60 completely degraded on 56 days of burial; however, SCBF-75 and SCBF-90 showed 85.76% and 69.22% biodegradation **(*Figure 7.10*(e)** and ***Figure 7.10*(j))**.

The lowered degradation rate of SCBF-90 is possibly due to presence of higher degree of thermally induced phosphate based cross-linkages. SCBF films were introduced into garden soil to examine effects of phosphorylation on biodegradability, change in physical appearance and subsequent weight loss was monitored upto 56 days (shown in ***Figure 7.10*****(a-e)**). As depicted in ***Figure 7.10*****(j),** SCBF-30, SCBF-45, SCBF-60, SCBF-75, and SCBF-90 demonstrated the most substantial degradation of 14.5%, 12.40%, 9.41%, 6.95%, and 0.35% at 7 day, respectively with no notable film disintegration. However, SCBF-30 and SCBF-45 films underwent disintegration within 14 days, leading to enhanced biodegradation of 27.83% and 19.66%, respectively. On other hand, SCBF-60, SCBF-75, and SCBF-90 showed lowered degradation of 17.28%, 8.92% and 5.39%, respectively with minor disintegration (***Figure 7.10*****(c)** and ***Figure 7.10*****(j)**). These findings suggest that phosphorylation does not modify intrinsic biodegradable properties of cellulose, however, the rate is controlled by degree of cross-linking. When SCBF films are buried in the soil, presence of moisture leads to their swelling, and microbial activity results in biodegradation of films [24,676,677]. The SCBF-30 demonstrated highest and most rapid degradation due to lower phosphate content, increased water absorption capacity, and reduced crosslinking.

7.2.12 LCA of SCBF-film

Figure 7.10**(f),** ***Figure 7.10*****(g),** and ***Figure 7.10*****(h)** depicts the environmental impacts resulting from the delignification, phosphorylation and production process of SCBF film. As illustrated in ***Figure 7.10*****(f),** the impact category of climate change (including and excluding biogenic carbon) exhibited the highest impacts, reaching 0.0198 kg CO_2 eq., surpassing all other categories. The primary factor contributing to the significant influence on climate change categories is likely attributed to the substantial release of greenhouse gases during electricity generation from hard coal.

The impacts generated in terrestrial ecotoxicity category was almost similar to the climate change category~0.0198 kg DB eq. The primary factor influencing these increased effects is utilisation of chemical reagents during pre-treatment, functionalization and processing of SB. Freshwater eutrophication and stratospheric ozone depletion exhibited the lowest impact values, measuring 1.45×10^{-8} kg P eq. and 3.63×10^{-8} kg CFC-11 eq., respectively. The LCA study suggests that environmental impacts resulting from treatment of SB waste are relatively less harmful and similar to the impact generated in traditional manufacturing of spray-deposited cellulose nanofiber films [331].

7.2.12.1 Normalization of mid-point results

The midpoint results obtained during the production of SCBF films were standardised to identify the dominant environmental impact categories. ***Figure 7.10*****(i)** demonstrates that among 18 categories, fossil depletion, photochemical ozone formation, and terrestrial acidification substantially contribute to the environmental impact. Fossil depletion exhibits the highest impact value, measuring 4.56×10^{-6} kg oil eq., while photochemical ozone formation and terrestrial acidification have impact values of 4.52×10^{-6} kg NO_x eq. and 3.22×10^{-6} kg SO_2 eq., respectively. The normalised midpoint results highlight fossil depletion, photochemical ozone formation, and terrestrial acidification as the dominant categories, and were subsequently chosen for sensitivity analysis.

7.2.12.2 Sensitivity analysis

A sensitivity analysis is conducted on predominant ecological categories associated with production of SCBF film to assess the variation in impact values on varying inputs of key factors. ***Table 7.1*** depicts effects of 10% increase and decrease of 8% in input values of key parameters, namely electricity, delignification, and phosphorylation on dominant environmental categories. Increase in electricity by 10%,

leads to proportional impacts in photochemical ozone formation (9.63%), terrestrial acidification (9.81%), and 10% fossil depletion. The primary cause of this phenomenon can be attributed to significant energy consumption associated with processes derived from the combustion of hard coal. A reduction of 8% in electricity input resulted in corresponding decreases by -7.84%, -7.69%, and -7.48% of fossil depletion, photochemical ozone formation, and terrestrial acidification, respectively. In addition, when the input of delignification were increased by 10%, impact values of fossil depletion, photochemical ozone formation, and terrestrial acidification increased by 5.09%, 5.38%, and 5.61%, respectively. Nevertheless, a reduction of 8% in input led to decrease of -4.13%, -3.85%, and -4.21% in impact of fossil depletion, photochemical ozone formation, and terrestrial acidification categories, respectively. Additionally, when the input of phosphorylation process were increased by 10%, there was a corresponding increase of 1.79%, 2.31%, and 1.87% in the impact values in the categories of fossil depletion, photochemical ozone formation, and terrestrial acidification, respectively. The sensitivity analysis conducted for the production of SCBF film reveals that electricity consumption emerges as the most crucial factor of significance. This phenomenon is apparent as the primary environmental categories display consistent fluctuations in response to proportional increments or decrements in electricity consumption during production.

Table 7.1 *Sensitivity analysis of the dominant environmental categories for transportation of butter in PET boxes.*

Categories	**Electricity**		**Delignification**		**Phosphorylation**	
	10% increase	8% decrease	10% increase	8% decrease	10% increase	8% decrease
FD	9.63	-7.84	5.09	-4.13	1.79	-1.65
PFO	10.00	-7.69	5.38	-3.85	2.31	-1.54
Terrestrial	9.81	-7.48	5.61	-4.21	1.87	-1.40

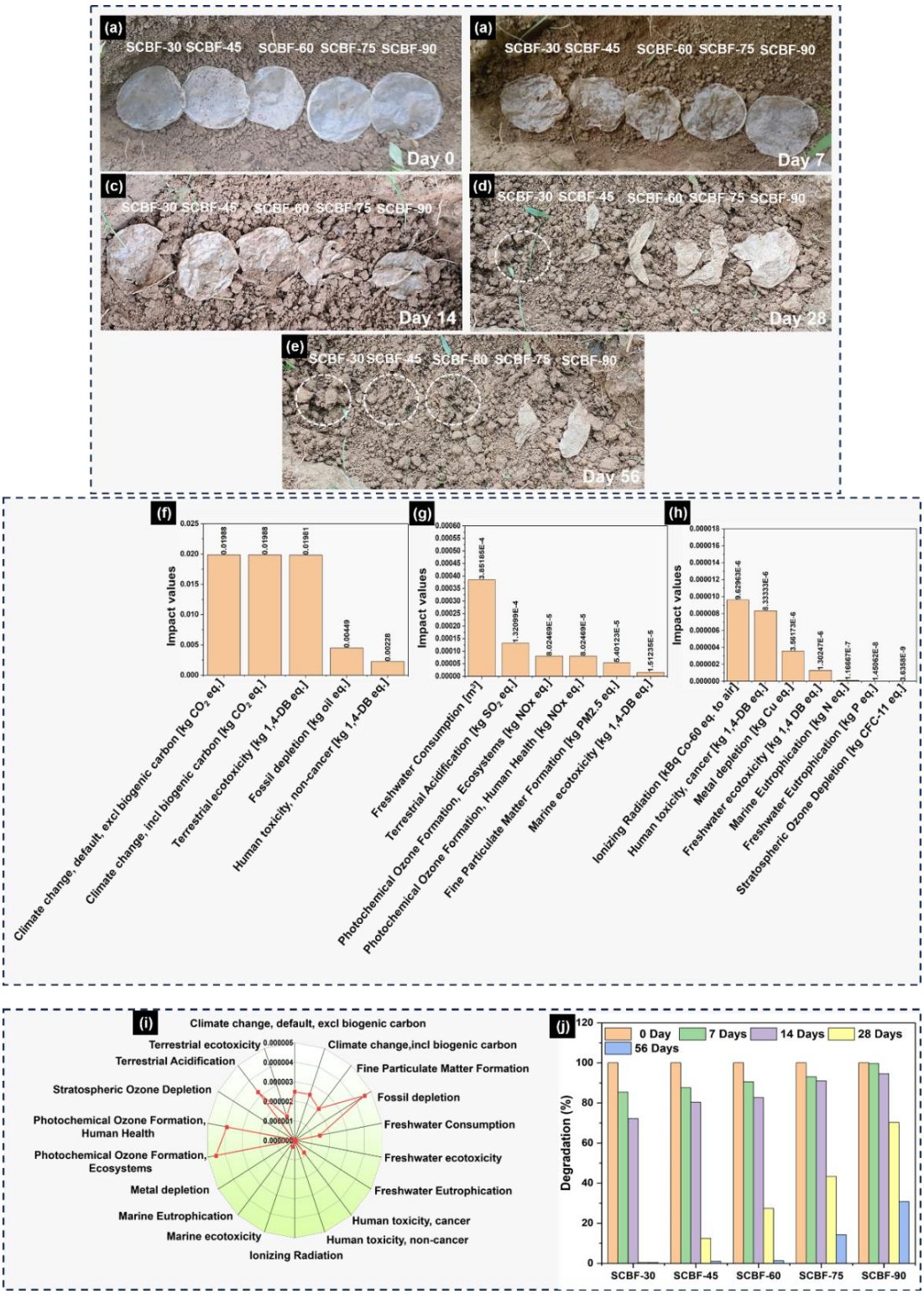

Figure 7.10 *Photographs of the films (a-e) sample taken to examine the physical changes occurring during different intervals of soil burial to study the process of biodegradation, (f-h) mid-point results generated from the production of single SCBF film, (i) normalisation of the mid-point results and (j) the graphs for the biodegradation percentage at different intervals of soil burial.*

7.3 Production of PSCB aerogel and Fruits foam

The present study focuses on conversion of abundantly available sugarcane bagasse (SB), a by-product of sugarcane processing industries, into aerogels/foams with commercial significance following a sustainable route. A scalable process utilizing low-cost agro-based chemicals through strategic delignification and phosphorylation route is reported. The developed aerogels were processed into foam-based products with interesting physio-chemical and structural characteristics of high porosity, ultra-lightweight, low density, mechanically strong with low thermal conductivity. Interestingly, the porous foams shows good insulation with high flame retardant properties compared to traditional non-degradable polyethylene or polyurethane-based foams (as shown in ***Figure 7.11***). The active packaging fruit foam nets developed in this study shows strong antioxidant, antibacterial properties and maintains structural integrity of packaged apples, providing a sustainable, low-cost, biodegradable and environmentally-friendly alternatives with commercial significance.

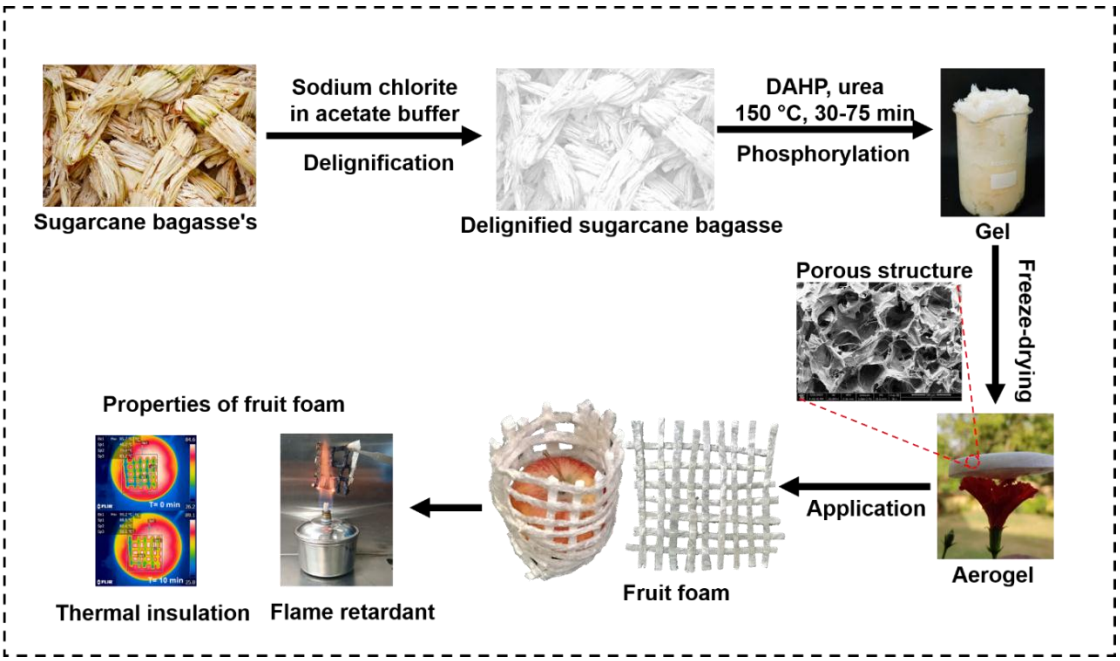

Figure 7.11 *Flow diagram depicting the production process of fruit foam, accompanied by a comprehensive overview of its properties.*

7.3.1 Functional properties: FTIR and XPS studies of phosphorylated SCB aerogels

FTIR analysis were performed in order to examine the changes in chemical functionalities and composition resulting from delignification and phosphorylation of SB. Both delignified and phosphorylated SB shows the presence of characteristic peaks of cellulose backbone of alkyl groups, stretching of C-O, carbonyl groups, vibrations of C-H bonds and -OH groups in the at the corresponding IR peaks of 830 cm^{-1}, 1025 cm^{-1}, 1653 cm^{-1}, 2855 cm^{-1} and 3280 cm^{-1} respectively, as depicted in ***Figure 7.12*****(a)** (21, 23,24, 25,26). The IR vibrational peak at 1153 in all the samples is mainly due to the C-O-C linkage of the glycosidic bond of cellulose [681]. The presence of IR-peaks at 1314 cm^{-1}, 1370 cm^{-1}, and 1420 cm^{-1} in all the samples corresponds to CH_2-wagging, C-H bending and CH_2 asymmetric bending of cellulose [682]. The presence of broad peaks around 2040-2150 is mainly ascribed to the H-O-H bond mainly due to the presence of moisture [683]. After phosphorylation, peaks at 920 cm^{-1} indicate the

presence of P-OH, confirming the phosphorylation reaction [34]. The presence of P-OH bonds in developed aerogels serves as evidence for successful phosphorylation of SB, which was further quantitatively evaluated through XPS and EDS spectroscopic studies. Full scan survey and high resolution XPS analysis corresponding to peaks of C1s, O1s and P2p of DSCB and PSCB-45 are presented in ***Figure 7.12*****.**

In the XPS survey**,** signals at binding energy (BE) ~532.08 eV, 285.08 eV and 133 eV represent the O1s, C1s and P2p of DSCB and PSCB-45 ***Figure 7.12*****((c)).** The deconvoluted P2p peaks in XPS analysis of PSCB-45 are present at BE of 133.08 eV, 133.9 eV, 132.8 eV, and 135.6 eV, indicating presence of P-O, PO_4^{-3}, P-C, and P=O bonds, respectively. However, only straight line with some noise were observed in the XPS spectra of DSCB confirming the absence of phosphate groups (***Figure 7.12*** **(d)).** On deconvolution, XPS peaks associated with the O1s electron orbitals in DSCB are observed at BE of 532.32 eV, 532.88 eV, and 530.5 eV which indicates the presence of O=C-OH, C-O-C, and C=O bonds, respectively [684–686]. The phosphorylation process in PSCB-45, resulted in the formation of O-C=O (at 532.2 and 533.6 eV) and O=C (at 530.52 eV) [687–689] bonds (***Figure 7.12*****(e))**. The detailed analysis of high-resolution C1s of DSCB, shows resolved peaks at BE~284.1 eV, 284.8 eV, 286 eV, and 286.8 eV indicating presence of distinct C=C, C-C, C-O, and C=O bonds, respectively [259,601,690,691]. The XPS spectrum of PSCB-45 reveals distinct peaks in C1s region at BE of 286.48 eV, 285.7 eV, 284.8 eV, and 284.15 eV corresponding to C-O-H, C-O-C, C-C, and C=C bonds respectively [692,693] (***Figure 7.12*****(f))**. The presence of C-P peaks in deconvoluted P2p and C1s spectra of PSCB-45 confirms the covalent grafting of phosphate groups on the cellulose backbone (21–23). The presence of

phosphate in PSCB-45 was 2.05 wt.% and 10.76 wt.%, confirmed by XPS and EDS analysis, which also confirms evidence of phosphorylation of DSCB.

7.3.2 Structural Properties of phosphorylated SCB aerogels

XRD analysis of DSCB and aerogels were carried out to understand the effect of various curing times on the crystal structures of cellulose phosphate (***Figure 7.12*(b))**.The deconvoluted XRD pattern of DSCB displays distinct peaks at 2θ~21.8° and 16.8°, corresponding to the crystalline planes (002) and (110) respectively representing cellulose I crystal structure [697]. On phosphorylation, XRD diffraction pattern of PSCB-30 and PSCB-45 shows shifted peaks to lowered 2θ~20.8° and 14.5°, which corresponds to crystal planes (110) and (101) respectively (43, 44). Further increasing the phosphorylation time, PSCB-60 and PSCB-75 exhibited two distinct peaks which further shifted to lowered 2θ~19.8° and 12.8°, attributed to crystal planes (002) and (101) respectively (45, 46). This shift of peaks to lowered angle indicates that covalent grafting of phosphate groups on cellulose chains during phosphorylation results in the alteration of crystal lattice structure with increase in crystal lattice parameters [701]. Further, evaluation of % crystallinity of DSCB was found to be~62.6%, which on phosphorylation shows gradual reduction in crystallinity with increased curing time for PSCB-30, PSCB-45, PSCB-60, and PSCB-75 to 42.5, 33.6, 27.8 and 22.7% respectively. Both shift in XRD patterns and reduction in crystallinity of developed aerogels, suggests that delignification and phosphorylation steps significantly affects the cellulose crystal structure and requires optimization in terms of curing time and temperature conditions.

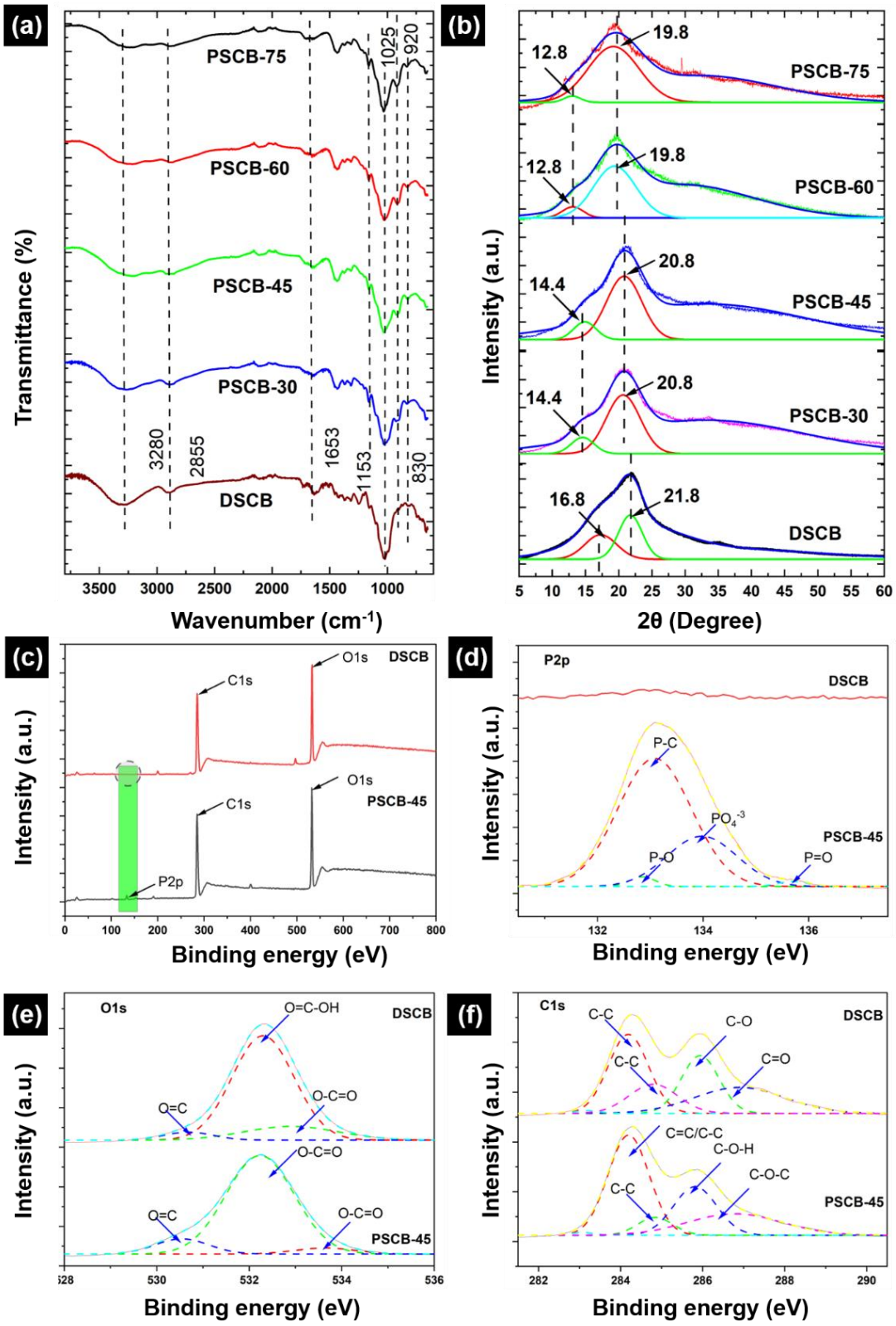

Figure 7.12 *(a) FTIR spectra, (b) XRD pattern, (c) XPS survey, broad spectrum and high-resolution XPS, (d) P2p, (e) O1s and (f) C1s of DSCB and PSCB-45.*

7.3.3 Morphological Properties of the foams

To understand the effect of phosphorylation and curing time on the morphology and dimension of cellulose phosphate fibers SEM observations at different magnification levels were carried out (as shown in ***Figure 7.13*****(a-i))**. The aerogels exhibit a highly distinct open porous microstructure with random distribution and presence of air voids. The microstructure within the aerogel originates from gradual growth of ice crystals at -20 °C during freezing, followed by sublimation step. This leads to conversion of ice to vapour leaving behind large pores, the dimension of which were found to be depend on the surface CC of PSCB. Notably, the pore distribution is not uniform across all synthesized Foams, potentially due to irregular ice crystal growth during freezing. The resulting microporous architecture of aerogels produced significantly contributes to their notable low thermal conductivity, light weight and improved water absorption capacity. ***Figure 7.13*****(i)** displays EDS analysis of PSCB-45 aerogel which indicates presence of phosphorous element by ~21.04 wt.% in line with XPS studies, confirming successful phosphorylation of PSCB with high CC.

7.3.4 Thermal properties

The thermal properties of all aerogels processed at different curing times were examined in order to explore the impact of phosphorylation on DSCB. According to thermograms (***Figure 7.14*****(a))** and data presented in ***Table 7.2***, the samples DSCB, PSCB-30, PSCB-45, PSCB-60, and PSCB-75 exhibited initial weight losses of 4.9%, 8.2%, 4.3%, 2.6%, and 5.2% respectively, within temperature range of 25-105 °C. The observed reductions in weight within the samples were primarily due to depletion of moisture or elimination of water molecules from surface that were bonded through hydrogen bonding [237]. In addition, a decrease of 10 wt.% for samples DSCB, PSCB-

30, PSCB-45, PSCB-60, and PSCB-75 were observed at temperatures of 238.6 °C, 205.8 °C, 205.8 °C, 218.9 °C, and 196.4 °C, respectively. The potential cause for early degradation or reduced thermal stability of phosphorylated aerogels compared to DSCB could be attributed to high phosphate CC as well as degradation of cellulose backbone during curing step. The grafted phosphate groups present in PSCB serves as catalysts initiating the early degradation leading to significant reduction in molecular weight of cellulosic backbone [652]. Furthermore, 50% degradation of DSCB, PSCB-30, PSCB-45, PSCB-60, and PSCB-75 were found to occur at 316.5°C, 421.2°C, 470.8°C, 499.9°C and 598.3 °C respectively. The potential cause for early degradation of PSCB below 400 °C could be attributed to depolymerization of glycosyl residues into volatile compounds were catalysed by the presence of high CC of phosphate residues [225]. Lastly, the char residue formed at 700 °C were found to be 8.3%, 33.7%, 41.3%, 44.1% and 47.3% for DSCB, PSCB-30, PSCB-45, PSCB-60, and PSCB-75 respectively. Increased char residue in produced aerogels compared to DSCB is due to the availability of phosphate groups which induces flame-retardant properties [225]. Therefore, it was observed that phosphorylation curing time significantly affects the surface charge, porosity, pore size and fibre dimensions which in turn affects the thermal conductivity, insulation and flame retardant properties, as discussed in subsequent sections.

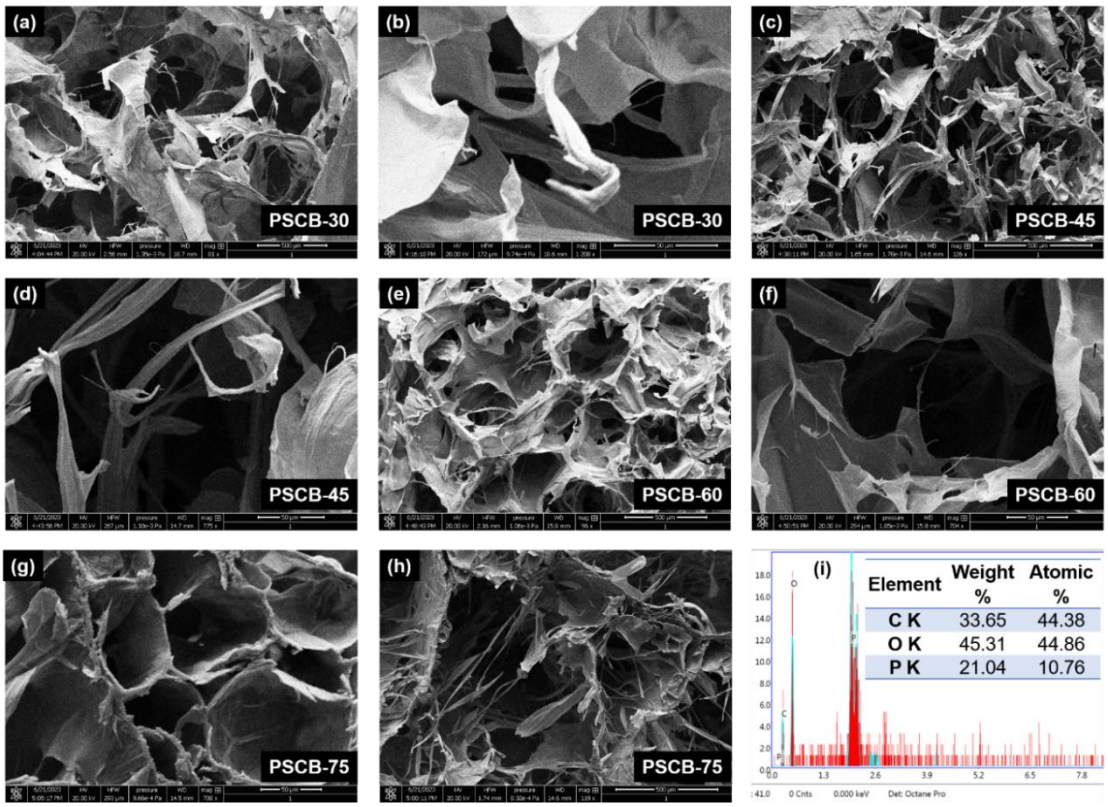

Figure 7.13 *SEM micrographs of (a-b) PSCB-30, (c-d) PSCB-45, (d-e) PSCB-60, (f-g) PSCB-75, and (h) EDS and corresponding elemental composition of PSCB-45.*

Table 7.2 *Thermal properties of developed aerogels processed at various curing times.*

Sample	T_{onset} (10% degradation, °C)	T_{50} (50% degradation temperature, °C)	Residual weight at 700 °C
DSCB	238.6	316.5	8.3
PSCB-30	205.8	421.2	33.7
PSCB-45	205.8	470.8	41.3
PSCB-60	218.9	499.9	44.1
PSCB-75	196.4	598.3	47.3

7.3.5 Thermal conductivity of the foams

The high porosity, low density combined with tuneable phosphate surface charge results in ultra-low thermal conductivity of developed aerogels which was measured at different temperatures. As shown in ***Figure 7.14*****(b),** aerogels has thermal

conductivities ranging in between 0.05-0.063 W/mK suggesting their exceptional insulation properties. Interestingly, the thermal conductivity was found to be depend on phosphate CC, which gradually increased with the curing time. Further, change in temperature didn't have any significant effect on thermal conductivities of developed aerogels, which slightly increased with rise in temperature from 30 to 50 °C. These suggests that changes in temperature don't bring any significant alterations in the morphology or porous architecture of the aerogels. Nevertheless, PSCB-30 shows the lowest thermal conductivities among all due to its notably high porosity of ~98% and porous network structure resulting in its outstanding insulating capabilities. The ultra-low thermal conductivity combined with improved phosphate charge makes developed flame-retardant aerogels potentially suitable for preservation of heat sensitive perishable fruits and vegetables contribute to prolonging their shelf-life.

7.3.6 Mechanical properties

***Figure 7.14*(c)** and ***Figure 7.14*(d)** evaluates the compressive strain-stress curve, providing insights into the mechanical stability of foam under both single and multiple cycles at different strains. ***Figure 7.14*(c)** shows the linear elastic deformation of PSCB-45 aerogels when subjected to longitudinal compression at applied strains of 30%, 60%, and 90%. It was observed that PSCB-45 aerogels under linear elastic deformation of 30%, shows a compressive strength of 0.0628 MPa. Further, on increasing the deformation to 60%, the compressive strength increases to 0.097 MPa and eventually reached an impressive 0.272 MPa on deformation of 90%. The increase in compressive strength of the aerogel is due to breakdown of porous structure and densification of foam's internal microstructure when subjected to higher strain. In addition, PSCB-45 aerogel was subjected to cyclic deformation of 5 cycles at applied strains of 30, 60, and

90%. As shown in ***Figure 7.14*****(d)**, under a strain of 30%, PSCB-45 aerogel demonstrated a compressive strength of 0.067 MPa, which after five strain cycles, shows a slight decrease to 0.062 MPa, and retaining its original shape and structure. Similar observations were made for 60% and 90% deformation, where the compressive stress of PSCB-45 aerogel very modestly decreased from 0.1 to 0.099 MPa and 0.27 MPa to 0.25 MPa on subjecting to 5 strain cycles. The evaluation of compressive strength of developed aerogels shows mechanical resilience, making it suitable for development of fruit foam nets required for maintaining the structural integrity of perishable fruits and vegetables.

7.3.7 Water uptake capacity

The effect of phosphate charge and degree of crosslinking on the water absorption capacity of developed foams were studied by immersing the aerogels in distilled water over 24 hours. According to ***Figure 7.14*****(f)**, PSCB-30 exhibited maximum water absorption capacity of 1826% compared to other aerogels developed. PSCB-45, PSCB-60, and PSCB-75 exhibited reduced water absorption capacities of 1671%, 1596%, and 1437% respectively. The increased water absorption capacity of PSCB-30 is possibly due to high phosphate CC which induces hydrophilic characteristics. Alternatively, reduction in water absorption capacity with the increased curing time is possibly due to cross-linking of the phosphate groups, as reported in earlier studies [77]. The presence of such crosslinks reduces the pore size as well as sites in which the water molecules could infiltrate the aerogel, improving its water stability making it suitable for potential food packaging applications.

7.3.8 Thermal insulation performance

The PSCB-45 aerogel was processed into fruit net foams to evaluate its thermal insulation qualities and compare it with commercially used polyethylene foams using an IR camera. The foam samples were placed directly on flat hot plate surface pre-heated at 90 °C and surface temperature of the foams were evaluated upto 1 hour. ***Figure 7.15*****(a)** illustrates that at t= 0 min, there was a temperature difference of 23.8 °C between the surface of hot plate and upper surface of polyethylene foam. However, after t=0, the temperature different between the hot plate surface and polyethylene foam ranges from 7.9 to 13 °C during entire experiment (**(*Figure 7.15*(c))**. However, in case of PSCB foam initially the temperature difference between surface of foam and hot plate is found to be~43.5 °C, which is evident from the blue coloured grid lines of net **(*Figure 7.15*(b))**. Nevertheless, the temperature difference between the surface of PSCB foam and hot plate decreased with time, however, the gradient remained significant enough until 1 hour. The difference in temperature between surface of PSCB foam and hot plate was measured to be 30.5°C, 27.4°C, 28.6°C, and 30.0 °C after 10, 20, 30, and 60 minutes, respectively **(*Figure 7.15*(b)** and ***Figure 7.15*****(c))**. The significant difference in the temperature profile is also evident from the presence of blue to greenish gridlines on fruit net with reddish hot plate in background. Based on these findings, it can be inferred that developed PSCB foam exhibits superior thermal insulation characteristics compared to the polyethylene foam, alongwith its interesting biodegradability characteristics makes it a sustainable alternative to fossil-fuel derived foams.

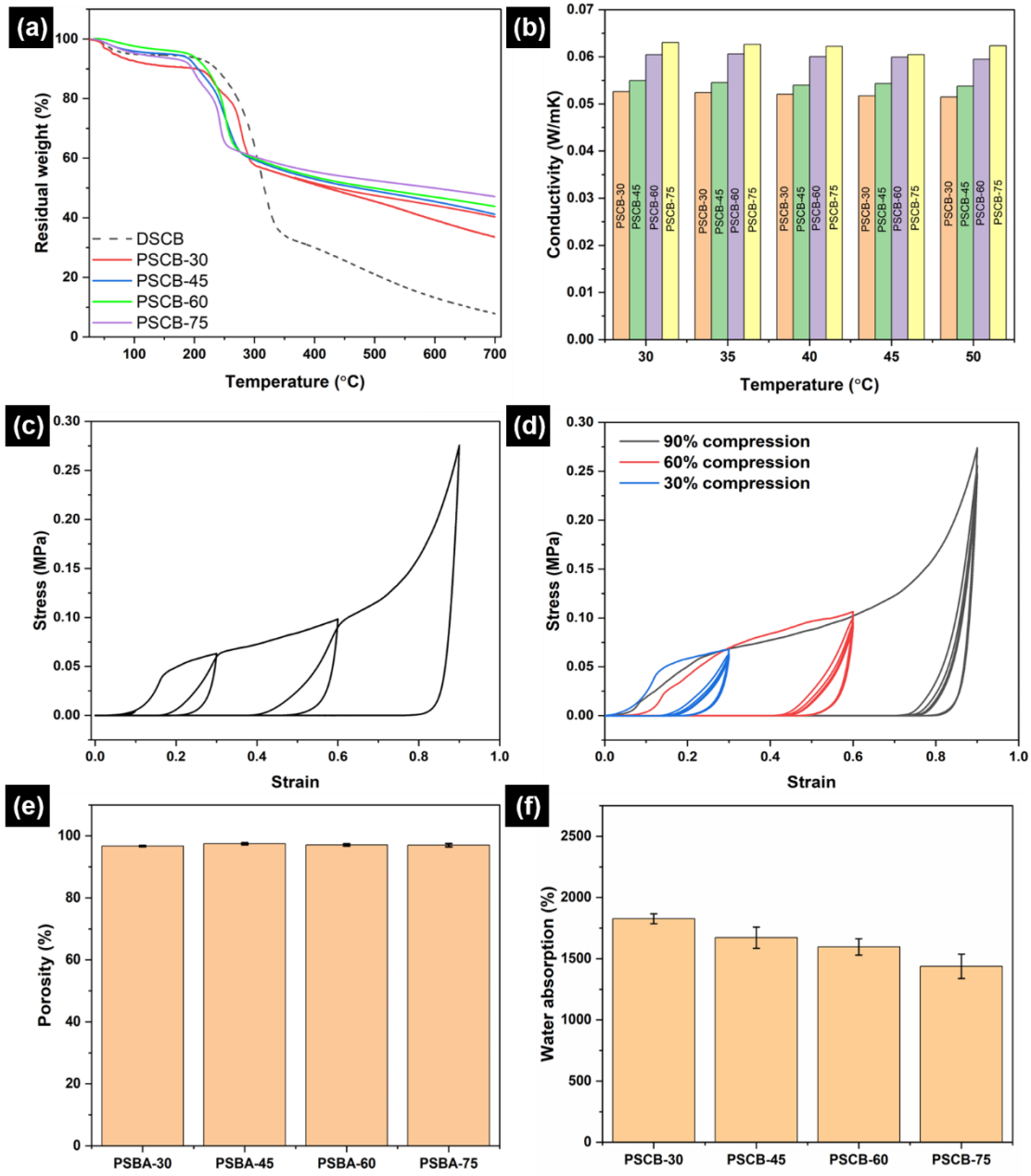

Figure 7.14 *(a) TGA, (b) thermal conductivity, (c) stress-strain curve of PSCB-45 in a single cycle, (d) multiple cycles, (e) porosity, and (f) water absorption capacity.*

7.3.9 Flame-retardant properties

The flame-retardant properties of developed foam were also evaluated and compared with commercially available polyethylene foam. As shown in ***Figure 7.15*****(d)**, PSCB aerogels showed strong flame-retardant properties against direct ethanol flame as it turns black when exposed to 70 seconds with generation of more than 40%

char residues. However, the commercially available polyethylene foams could not even withstand the flame for six seconds (***Figure 7.15*(e)).** These results demonstrate that the developed foam from phosphorylated SCB have excellent flame retardancy. PSCB has a highly efficient flame-retardant effect due to the formation of a carbon residue char layer, which interestingly maintains its structural stability even after complete combustion (50, 51).

7.3.10 Packaging of apples

Usually, fruits and vegetables are susceptible to damage once they are harvested, particularly during transportation, because of the mechanical shock that occurs during the process. Exposure of fruits to mechanical stress can result in structural damage, subsequently leading to the loss of moisture and prone to microbial growth. This degradation affects the quality of the fruit and raises concerns about its safety during post-harvest handling. This study developed PSCB-G foam specifically for packaging of apples, and evaluation of their ability to withstand the mechanical stress. The developed PSCB-G foam demonstrated exceptional flexibility **(*Figure 7.16*(a)** and ***Figure 7.16*(b))**, making it highly suitable for easily enveloping fruits (***Figure 7.16*(c)** and ***Figure 7.16*(d)**). ***Figure 7.16*(e)** demonstrates that applying stress directly to the apple resulted in early damage occurring at a strain of 20%. Nevertheless, the polyethylene foam and PSCB-G foam (***Figure 7.16*(e)** and ***Figure 7.16*(f)**) exhibit no detrimental effects when subjected to the same applied stress level. The maximum stress that the apple could withstand was 0.191 MPa. On using polyethylene foam and PSCB-G foam as wrap over apple, the stress levels decreased to 0.156 and 0.089 MPa, respectively, at shear strain of 20% (***Figure 7.16*(f)**. The findings suggest that developed aerogel foam can efficiently protect apple against mechanical shocks,

thereby, protecting against damage and spoilage. Alongwith it PSCB foam has exceptional thermal insulation characteristics, efficiently protecting the apple from heat or the fluctuations in the temperature profile. The developed foam with improved flame-retardant properties, thermal insulation and mechanical strength makes it suitable for storage and preservation of perishable fruits and vegetables.

7.3.11 Anti-oxidant properties

Through the incorporation of antioxidants into packaging materials, the detrimental effects of oxidative degradation can be greatly reduced. This is particularly beneficial for preserving products that are prone to deterioration, such as fruits. Integration of antioxidants into packaging materials, is gaining popularity as a feasible substitute for directly infusing antioxidants into packaged products [704]. This procedure mitigates any potential issues associated with modifications in the product's taste, aroma, or visual characteristics [705]. Therefore, in this study gallic acid as an antioxidant material have been incorporated into the gel for incorporation antioxidant properties. Gallic acid is natural compounds containing large number of hydroxyls groups which impart antioxidant properties. Therefore, the antioxidant properties of the PSCB-G foam, polyethylene foam and PSCB were evaluated *via* DPPH free radical scavenging method. The result present in the ***Figure 7.16*****(g)**, demonstrate that the foam without gallic acid showed 13.8% which improved to 88.1% with gallic acid incorporated sample. However, no antioxidant properties were observed in the polyethylene foam. This finding shows potential for reducing oxidative degradation in packaged goods, especially fruits, without affecting their sensory attributes.

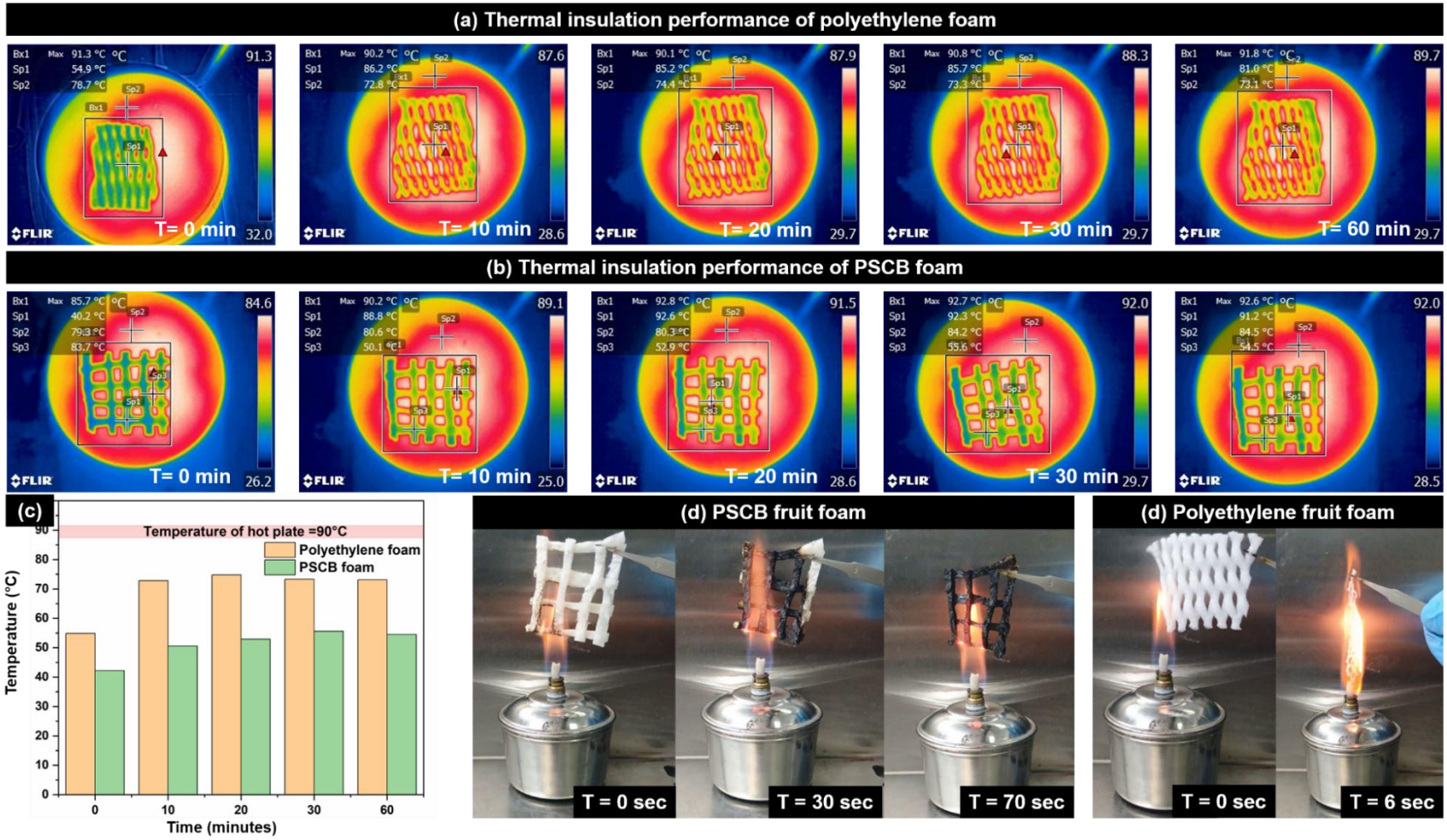

Figure 7.15 *Illustrates the thermal insulation properties of (a) polyethene foam, (b)PSCB foam, (c) temperature profile of the foams and hot plate surface, flame-retardant properties of (d) PSCB foam, and (e) commercial polyethylene foam.*

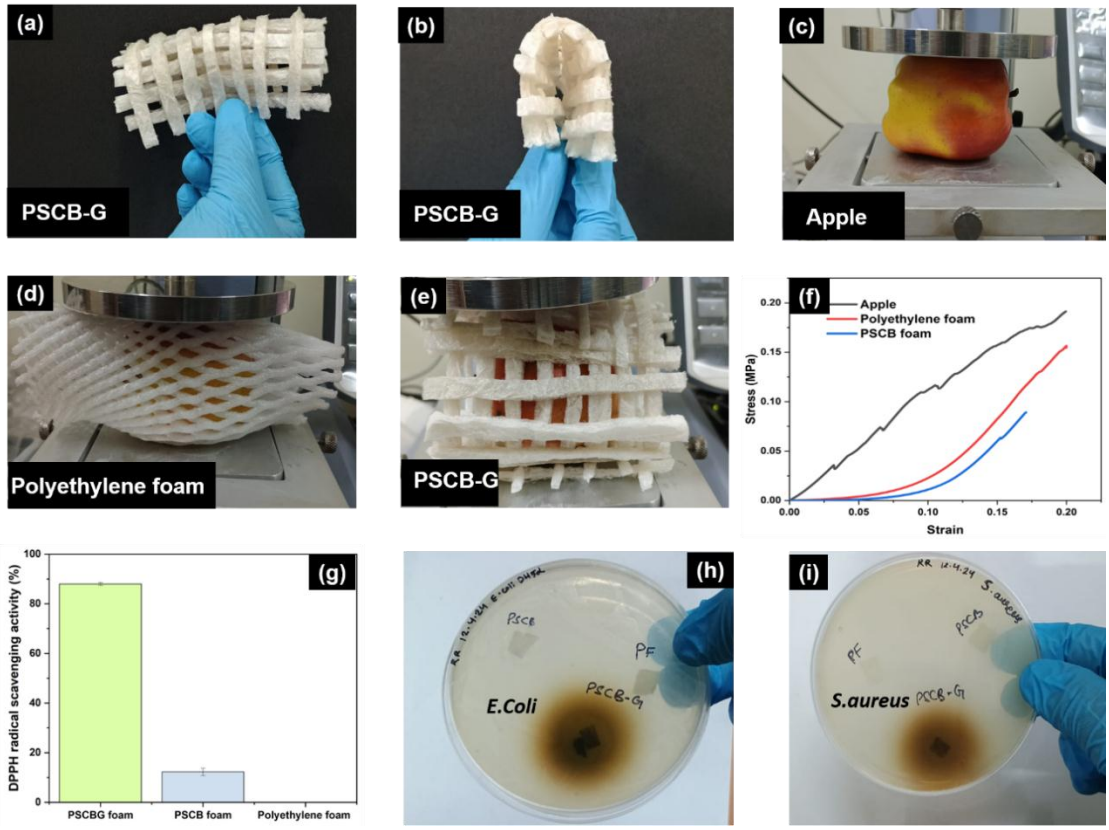

Figure 7.16 *(a) Photograph of an apple wrapped in PSCB-G foam, (b-c) Photographs showcasing the flexibility of PSCB-G foam; (d) Photograph of an apple packaged in polyethylene foam, (e) Photograph displaying the unpackaged apple, (f) Photograph of an apple packaged in PSCB-G foam, (g) Stress-strain curve comparing apple, polyethylene foam, and PSCB-G foam covered apple, (h) Evaluation of antioxidant properties.*

7.3.12 Antibacterial activity

The antibacterial efficacy of PSCB foam containing gallic acid (PSCB-G), PSCB, and polyethylene foam were assessed against the Gram-positive bacteria *S. aureus* ***Figure 7.16(i)*** and the Gram-negative bacterium *E. coli*. ***Figure 7.16*****(h)** demonstrates that the addition of gallic acid to the PSCB foam resulted in antibacterial effects against both *E. coli* and *S. aureus*. The PSCB-G exhibited a zone of inhibition measuring 9 mm on nutrient agar against *E. coli*, and 14 mm against *S. aureus*. However, no zones of inhibition were observed for PSCB and polyethylene foam.

7.4 Summary

The chapter explores innovative approaches to valorize SB by transforming it into valuable products with diverse applications. Two main studies are conducted, each focusing on distinct transformation methodologies and resulting products. In the first study, waste SB is converted into phosphorylated gels and packaging films, addressing the issue of improper disposal methods while creating environmentally friendly packaging materials. The gels exhibit transparency, mechanical robustness, flame-retardancy, flexibility, thermal stability, and biodegradability. These properties make them suitable for packaging applications, demonstrated by the extension of paneer shelf-life by up to 14 days without pathogenic bacteria growth at refrigerated temperatures. Additionally, life cycle assessment (LCA) confirms lower carbon dioxide emissions, endorsing the sustainability of the production process. This study highlights the potential of SB as a substitute for petroleum-based plastics in packaging, contributing to waste reduction and environmental preservation. In the second study, SB is transformed into aerogels and fruit foam through delignification, phosphorylation, and freeze-drying techniques. The resulting aerogels possess exceptional properties such as high porosity, low thermal conductivity, low density, and impressive mechanical strength. Incorporating gallic acid enhances antibacterial activity and free radical scavenging ability, while the fruit foam demonstrates outstanding flame-retardant characteristics and thermal insulation properties. Utilizing the fruit foam for packaging effectively reduces stress levels on packaged goods. This study suggests a promising and eco-friendly alternative for food packaging, addressing environmental concerns associated with traditional plastic packaging materials. Overall, both studies demonstrate the potential of SB valorization in producing

valuable, environmentally friendly products with diverse applications, contributing to sustainability and waste reduction in the agricultural and packaging industries.